Optical Transition Radiation Imaging of Intense Proton Beams at FNAL

Victor E. Scarpine, Alex H. Lumpkin, Warren Schappert, and Gianni R. Tassotto

***Abstract*—Initial results are presented of a prototype optical transition radiation (OTR) detector under development at Fermi National Accelerator Laboratory. The purpose of this prototype detector is to evaluate the feasibility of using OTR imaging of intense proton (or antiproton) beams in transport lines for beam position and shape measurements. A secondary purpose is to develop experience in designing, constructing and operating a camera and optics system in high radiation environments. Measurements are made of 120 GeV proton beams with intensities up to 4.7×10^{12} particles. Data are presented of OTR with titanium and aluminum foils.**

***Index Terms*—120-GeV protons, optical transition, radiation proton.**

I. Introduction

PARTICLE-BEAM diagnostic techniques based on optical transition radiation (OTR) have been demonstrated at a number of facilities over a wide range of beam energy (or Lorentz factor, gamma) [1]–[3]. The Fermi National Accelerator Laboratory (FNAL) is pursuing a number of projects where either beam luminosity for the Tevatron collider (Run II) or proton intensity for neutrino experiments require careful tracking of beam properties, such as transverse profile and shape (tilt), transverse position, emittance and intensity, throughout the facility. The feasibility of using OTR imaging for the relatively low Lorentz factor ($\gamma \sim 129$) intense proton beams at FNAL is based on a comparison with high Lorentz factor electron-beam results at the Advanced Photon Source (APS) linac [3] and proton-beam results at CERN [2]. This comparison suggests that significant levels of OTR will be generated by the generally lower Lorentz factor but higher intensity ($\sim 4.5 \times 10^{12}$ particles) proton beams at FNAL [4].

Optical transition radiation is generated when a charged particle transits the interface between two media with different dielectric constants (e. g., vacuum to dielectric or vice versa) [2], [5]. The effect is a surface phenomenon that can be understood as the collapsing of the electric dipole formed by the approaching beam charge and its image charge in the dielectric at the surface. As the fields readjust, a pulse of radiation is emitted. This radiation is emitted over the visible spectrum so optical imaging techniques can be used to acquire the OTR signal and then reconstruct beam size and position at the dielectric. The single-particle spectral angular distribution of the number of photons, N, per unit frequency (ω) and solid angle $(\mathrm{d}\Omega)$ is given by [5], [6]

$$\frac{d^2N}{d\omega d\Omega} = \frac{2e^2}{\pi h c \omega} \frac{(\theta_x^2 + \theta_y^2)}{(\gamma^{-2} + \theta_x^2 + \theta_y^2)^2} \tag{1}$$

where e is the electron charge, h is Planck's constant, c is the speed of light, γ is the Lorentz factor of the charged particle, and θ_{x} and θ_{y} are the angles from the OTR emission axis. For the forward OTR this axis is the same as the particle beam while for the backward OTR this axis is the specular reflection axis. In addition, the intensity of the backward OTR is proportional to the reflectivity of the surface. This expression shows that the angular distribution is maximum at $\theta \sim 1/\gamma$.

Since OTR is a surface phenomenon, thin foils are used as the converter to reduce beam scattering and minimize heat deposition.

II. Prototype OTR Detector

We have constructed and installed a prototype OTR detector at FNAL. The prototype is located in an air gap in the AP1 transport line upstream of the antiproton production target. This beamline transports 120 GeV protons with intensities up to 4.7×10^{12} particles in a 1.6 μs spill at a rate of one spill every 2 s. Beam intensities are measured with a toroid with an accuracy of about one percent. At this location the rms transverse beam size is a few millimeters and the OTR angular distribution $(1/\gamma)$ is ~ 8 milliradians. In addition, the long-term survival of two titanium vacuum windows on either end of the air gap establishes that an OTR foil will survive the beam intensities at this location.

The detector uses either a 12 μm titanium or 20 μm aluminum foil in the air gap at 45° with respect to the beam that serves as the OTR generator screen. The foil mount has the ability to tilt in order to match the OTR specular reflection axis to the detector optical axis. A lens system collects the OTR generated in a cone of radius $2/\gamma$ about the optical axis and focuses it on to a charge injection device (CID) camera. The CID camera is a standard RS-170 format and operates at 30 image frames per second. The camera is mounted on a translation stage that allows for focus adjustment. The optics operates at a magnification of $1/9$ and produces an equivalent pixel size of approximately 100 μm by 100 μm at the foil or an 80 mm by 55 mm field of view.

Manuscript received October 29 2003. This work was supported by the U.S. Department of Energy under Contract DE-AC02-76CH03000 and Contract W-31–109–ENG-38.

V. E. Scarpine and G. R. Tassotto are with the Fermi National Accelerator Laboratory, Batavia, IL 60510 USA (e-mail: scarpine@fnal.gov; tassotto@fnal.gov).

A. H. Lumpkin is with the Argonne National Laboratory, Argonne, IL 60439 USA (e-mail: lumpkin@aps.anl.gov).

W. Schappert was with the Fermi National Accelerator Laboratory, Batavia, IL 60510 USA. He is now with Array Systems Computing Inc., Toronto, ON M3J-3H7, Canada (e-mail: warren@array.ca).

Digital Object Identifier 10.1109/TNS.2004.832904

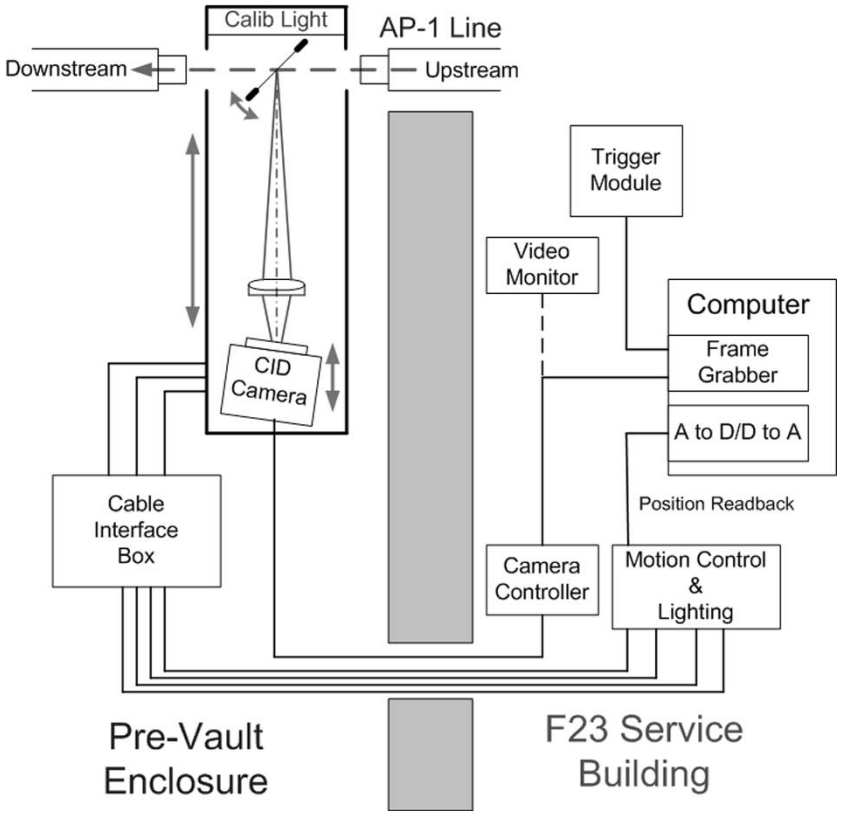

Fig. 1. Block diagram of the prototype OTR detector system.

To maintain focus over the foil, the camera is mounted at an angle to satisfy the Scheimpflug condition [7]. Images of OTR are acquired and saved to a computer using a standard frame grabber card. Camera light levels are controlled by the use of selectable neutral density filters. Fig. 1 shows a block diagram of the prototype OTR detector system. For operational purposes, the entire OTR detector can be moved out of the AP-1 transfer line. Foil, camera and detector motions are controlled remotely via a control box or computer.

The multiple titanium vacuum foils at this location produce a high radiation environment. Because of this radiation, the camera and optics are placed approximately one meter from the OTR foil. At this location, the CID camera and optics receive $\sim$6 kRad/week. The CID camera has been shown to operate beyond a total dose over 1 MRad [8].

Both aluminum and titanium foils are tested since each has distinct advantages. Aluminum has a higher reflection coefficient but titanium is stronger and has a higher melting point. For future OTR detectors, the choice of foil material will depend on beam intensity and beam size.

III. Optical Calibration

We have integrated a simple optical calibration system into the prototype OTR detector to measure image scale and focus. Fiducial holes are placed at precise locations in the foil near the corners of the field of view. These holes are then back illuminated and imaged. Images over a range of camera positions allow the best focus to be determined. Fig. 2 shows a grayscale image of the fiducial holes at nominal focus. Image calibration

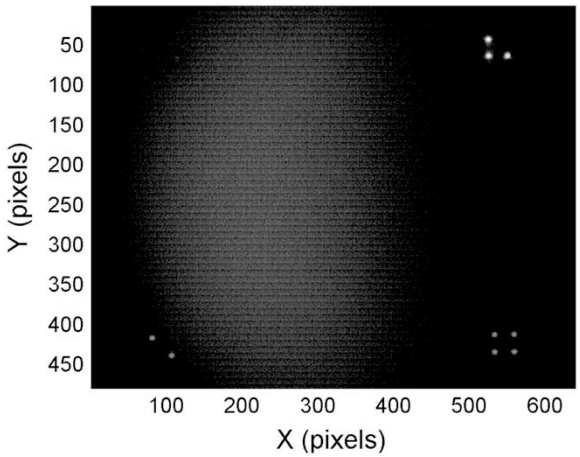

Fig. 2. Grayscale image of fiducial holes in 12 μm titanium foil. The location of fiducials allows the image scale to be determined while the fiducial sharpness allows the best focus to be determined.

gives an X scale of 123 μm per image pixel and a Y scale of 106 μm per image pixel.

IV. OTR Beam Images

Measurements have been made of the OTR signal generated by 120 GeV proton beams for both titanium and aluminum foils up to an intensity of 4.7×10^{12} particles/spill. Since initial images taken with no light attenuation saturate the CID camera, some degree of light attenuation is required. All OTR images presented here have been filtered with a 5×5 median filter to reduce noise artifacts.

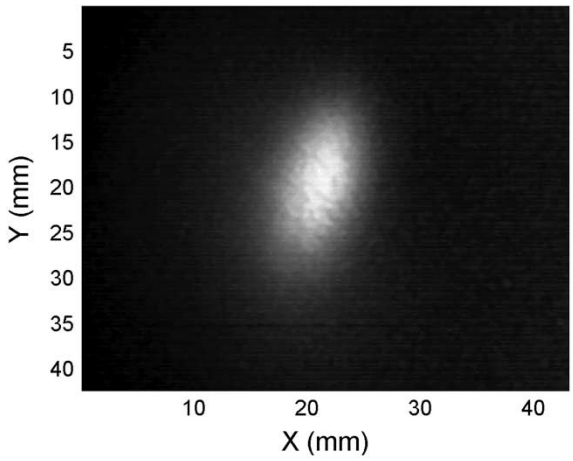

Fig. 3. Grayscale OTR image from 4.5×10^{12} 120 GeV protons through 12 μm titanium foil. Light intensity is attenuated by a factor of 200 to avoid camera saturation.

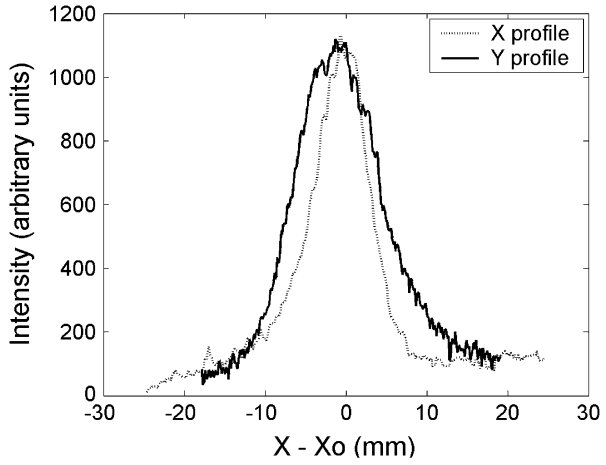

Fig. 4. Horizontal and vertical line profiles of OTR light intensity taken through the maximum of the OTR distribution relative to the peak intensity position, $\mathrm{X_O}$.

A. OTR Measurement With Titanium

Fig. 3 shows a grayscale backward OTR image from 4.5×10^{12} 120 GeV protons through 12 μm titanium. Optical transition radiation is attenuated by a factor of 200 in order to avoid camera pixel saturation. This image shows a clear indication that the transverse beam shape is tilted at this location in the AP-1 transfer line. Fig. 4 shows vertical and horizontal line profiles of light intensity relative to the peak intensity position, $\mathrm{X_O}$, after correction for image distortion. These profiles indicate a full-width at half-maximum of $\sim$8 mm in x and $\sim$12 mm in y.

B. OTR Shape Measurement

Fig. 5 shows a grayscale backward OTR image from 1×10^{12} 120 GeV protons through 12 μm titanium for a nominal beam size. Fig. 6 shows a similar beam where the vertical size has been reduced by a factor of $\sim$2. For both images the OTR light has been attenuated by a factor of 200. These images show that the prototype detector tracks the change in the beam shape.

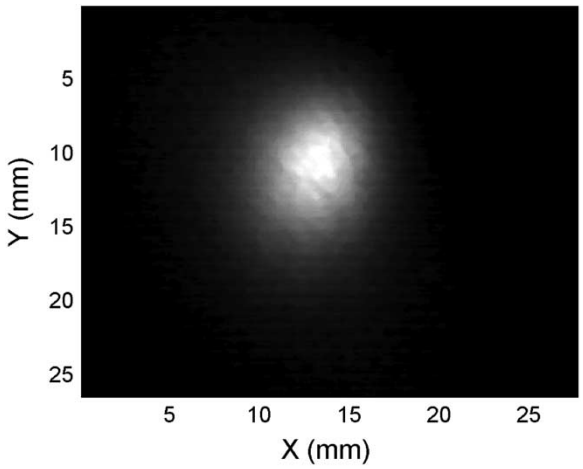

Fig. 5. Grayscale OTR image from 1×10^{12} 120 GeV protons through 12 μm titanium foil at nominal beam size.

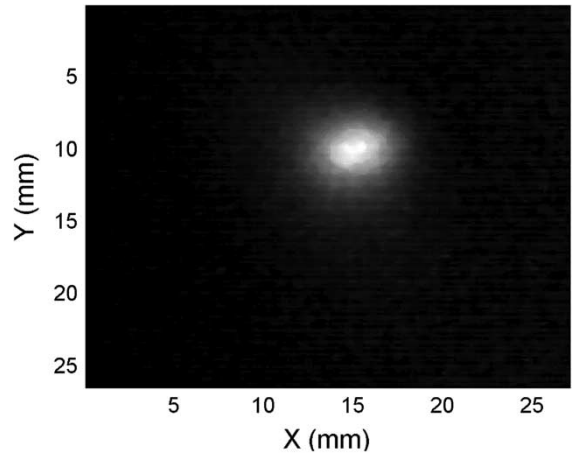

Fig. 6. Grayscale OTR image from 1×10^{12} 120 GeV protons through 12 μm titanium foil with a factor of $\sim$2 reduction in vertical beam size.

C. OTR Position Measurement

Fig. 7 shows OTR images taken with three different vertical beam positions for different spills. The images are from 1×10^{12} 120 GeV protons through 12 μm titanium. The images track the change in beam position and measure a beam position of $+11.1$ mm and -11.1 mm from nominal center beam position. Adjacent rf beam position monitors measure beam positions of $+10$ mm and -10 mm from nominal center. The difference in these measurements is not understood at this time.

The left and center images in Fig. 7 have similar beam size and shape while the right image appears to have a different beam shape. It is not clear if this is a real beam effect or a shape induced by the titanium foil. Further measurements are needed to understand this effect.

D. OTR Measurement With Aluminum

Fig. 8 shows a grayscale backward OTR image from 4.7×10^{12} 120 GeV protons through 20 μm aluminum with a factor of 1000 light attenuation. As described above, backward OTR is proportional to the reflectivity of the foil and aluminum has

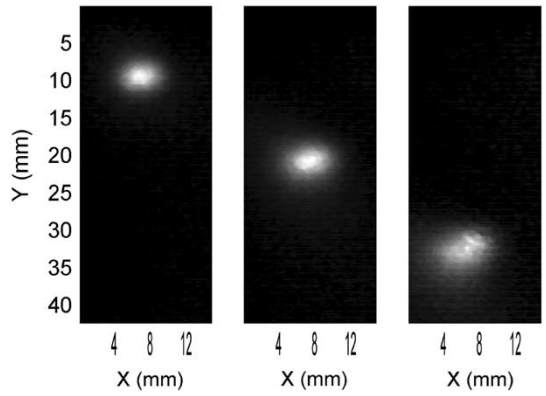

Fig. 7. Grayscale OTR images from 1×10^{12} 120 GeV protons through 12 μm titanium for different beam positions. The center image is taken at nominal beam position. The left image is taken at $+10$ mm vertical displacement from nominal and the right image is taken at -10 mm vertical displacement as measured by rf beam position monitors.

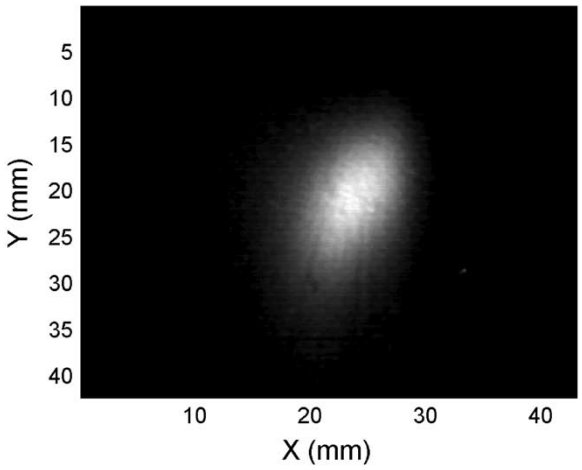

Fig. 8. OTR from 4.7×10^{12} 120 GeV protons through 20 μm aluminum foil with a factor of 1000 light attenuation.

a higher reflectivity than titanium. A factor of 1000 light attenuation for aluminum versus 200 for titanium shows that we are seeing more OTR from the aluminum foil. In addition, similar OTR size and shape from titanium (Fig. 3) and aluminum (Fig. 8), for similar beam conditions, indicate that the foils are not introducing artifacts into the image.

V. Conclusion

We have developed and installed a prototype OTR detector and have taken first images with 12 μm titanium and 20 μm aluminum foils. Measurements indicate that OTR light levels are strong enough to allow imaging at particle intensities as low as 5×10^9 120 GeV protons for a beam size of $\sim$1 mm rms or smaller. Larger beam sizes can be imaged with proportionally higher beam intensities.

Examination of the titanium foil after $\sim 7 \times 10^{17}$ 120 GeV protons shows no surface changes, but long-term damage to foils, camera and optics have not been measured.

Optical transition radiation images obtained from this prototype suggest that OTR detectors can be used for high-intensity proton beams. Possible OTR applications for FNAL include developing 1) a three-foil beta function matching station in each of the transport lines between the Main Injector and the Tevatron to measure both protons and antiprotons, 2) a beam profiling station for the high-intensity 120 GeV transport lines for the NuMI project, 3) a beam profiling station for the 8 GeV transport lines, 4) a beam halo detector, 5) a single bunch detector with a gated, intensified camera, and 6) an OTR detector located in the Tevatron for injection studies.

Acknowledgment

The authors would like to thank their colleagues in the FNAL Beams Division for their contributions to the development, integration and testing of our prototype OTR detector, including E. Lorman, J. Morgan, T. Leveling, and E. Harms; C. Lindenmeyer, J. Korienek, R. Miksa, K. Kephart, and W. Newby of FNAL Particle Physics Division for their outstanding work in the mechanical design and construction of the detector; G. Ferioli (CERN) for conversations on OTR detectors; and S. Pordes (FNAL) and B. Webber (FNAL) for their enthusiasm and encouragement for pursuing OTR detectors.

References

[1] P. Goldsmith and J. V. Jelley, "Optical transition radiation from protons entering metal surfaces," *Phil. Mag.*, vol. 4, pp. 836–844, 1959.

[2] J. Bosser, J. Mann, G. Ferioli, and L. Wartski, "Optical transition radiation proton beam profile monitor," *Nucl. Instrum. Meth.*, vol. 238, pp. 45–52, 1985.

[3] A. H. Lumpkin, B. X. Yang, W. J. Berg, M. White, J. W. Lewellen, and S. V. Milton, "Optical techniques for electron-beam characterizations on the APS SASE FEL project," *Nucl. Instrum. Methods*, vol. A429, pp. 336–340, 1999.

[4] A. H. Lumpkin and V. Scarpine, "The feasibility of OTR imaging of high-intensity proton beams at FNAL," presented at the *Proc. Particle Accelerator Conf.*, Portland, OR, May 12–16, 2003.

[5] L. Wartski, J. Marcou, and S. Roland, "Detection of optical transition radiation and it's application to beam diagnostics," *IEEE Trans. Nucl.Sci.*, vol. 20, pp. 544–548, June 1973.

[6] D. W. Rule, R. B. Fiorito, and W. D. Kimura, "The effect of detector bandwidth on microbunch length measurements made with coherent transition radiation," in *Advanced Accelerator Concepts: Eighth Workshop*, W. Lawson, C. Bellamy, and D. Brosius, Eds., 1999, vol. AIP 472, pp. 745–754.

[7] W. J. Smith, *Modern Optical Engineering*, 2nd ed. New York: McGraw-Hill, 1990, p. 52.

[8] J. Carbone, J. Zarnowski, M. Pace, S. Czebiniak, and R. Carta, "Megarad and scientific CIDs," *Proc. SPIE*, vol. 2654, pp. 131–138, 1996.